Femtosecond Enhancement Cavities in the Nonlinear Regime

S. Holzberger,[1,2,*] N. Lilienfein,[1,2] H. Carstens,[1,2] T. Saule,[1,2] M. Högner,[1,2] F. Lücking,[2] M. Trubetskov,[1] V. Pervak,[2] T. Eidam,[3] J. Limpert,[3] A. Tünnermann,[3] E. Fill,[1,2] F. Krausz,[1,2] and I. Pupeza[1,2]
[1]*Max-Planck-Institut für Quantenoptik, Hans-Kopfermann-Straße 1, 85748 Garching, Germany*
[2]*Ludwig-Maximilians-Universität München, Am Coulombwall 1, 85748 Garching, Germany*
[3]*Friedrich-Schiller-Universität Jena, Institut für Angewandte Physik, Albert-Einstein-Straße 15, 07745 Jena, Germany*
(Received 30 December 2014; published 8 July 2015)

We combine high-finesse optical resonators and spatial-spectral interferometry to a highly phase-sensitive investigation technique for nonlinear light-matter interactions. We experimentally validate an *ab initio* model for the nonlinear response of a resonator housing a gas target, permitting the global optimization of intracavity conversion processes like high-order harmonic generation. We predict the feasibility of driving intracavity high-order harmonic generation far beyond intensity limitations observed in state-of-the-art systems by exploiting the intracavity nonlinearity to compress the pulses in time.

DOI: 10.1103/PhysRevLett.115.023902 PACS numbers: 42.65.Ky, 42.60.Da, 52.38.-r

During light-matter interactions, the properties of the light field are subjected to changes reflecting the physical mechanisms underlying the interaction and revealing fundamental properties of matter. A powerful tool for high-precision studies of light-matter interactions is the passive optical resonator, also known as enhancement cavity (EC). An EC can be resonantly excited by laser light, resulting in an enhancement of the input power and of the single-round-trip phase by up to several orders of magnitude. ECs have been successfully employed for high-sensitivity measurements of absorption [1] and of dispersion [2,3] in the linear regime. Here, we present the first quantitative study of the nonlinear phase associated with the propagation of an ultrashort laser pulse through a nonlinear medium exploiting the sensitivity enhancement of more than 2 orders of magnitude provided by an EC.

In the last decade, the advent of high-power femtosecond lasers and the design of adequate ECs have enabled ultrashort pulses with an otherwise unattainable combination of peak intensities and average powers [4]. The most prominent application has been high-order harmonic generation (HHG) in an intracavity gas target, at repetition rates exceeding 10 MHz [5–9]. Although cavity-enhanced HHG has matured to deliver phase-stable extreme-ultraviolet (XUV) frequency combs enabling first spectroscopic experiments [7,8], all state-of-the-art EC-HHG systems suffer from a saturation behavior of the intracavity intensity with respect to the input peak power, referred to as *intensity clamping* [9–12]. Currently, this severely limits the further scaling of the photon flux and of the XUV photon energies attainable with this technology and questions its applicability to other nonlinear conversion processes. The models developed so far [11,12] capture the main physical mechanisms of this limitation qualitatively but do not allow for accurate quantitative predictions, such that optimizing the cavity design with respect to the nonlinear conversion remains an open challenge.

In this Letter, we use the phase sensitivity of a high-finesse EC—the very effect responsible for the intensity clamping—to precisely study the nonlinear interaction of a laser pulse with a gas target. The full pulse characterization in the spectral domain allows for the formulation of a quantitative, *ab initio* nonlinear propagation model, experimentally validated in a wide range of the critical parameters. Second, we use this model to derive a scaling law quantitatively describing the intensity-clamping behavior in ECs employing mirrors according to the *standard approach* used in all setups reported so far, i.e., a uniform spectral reflectivity, symmetric with respect to the input spectrum. This analytic expression enables the optimization of the nonlinear conversion efficiency in standard-approach ECs. Third, we address the question of whether or not nonlinear ECs can be operated beyond the intensity limitations exhibited by the standard approach. We demonstrate that the ionization-induced spectral broadening in conjunction with cavity mirrors with tailored reflectivity can be used to dramatically compress the intracavity pulse in time, while maintaining a high power enhancement factor. This finding represents the first viable route towards significantly surpassing the intensity limitations of state-of-the-art nonlinear ECs and, therefore, reveals an enormous new potential of the EC technology for building high-power, broadband, coherent sources in spectral ranges where suitable laser materials are absent, such as the XUV, the midinfrared, and the THz ranges.

The experimental setup is depicted in Fig. 1. The chirped-pulse-amplification-based Yb-fiber laser system has been previously described in Refs. [2,13]. It delivers a 77-MHz train of near-Fourier-limited 180-fs pulses carried at a wavelength of 1040 nm. The pulses can be linearly chirped to 640 fs, or spectrally broadened in a

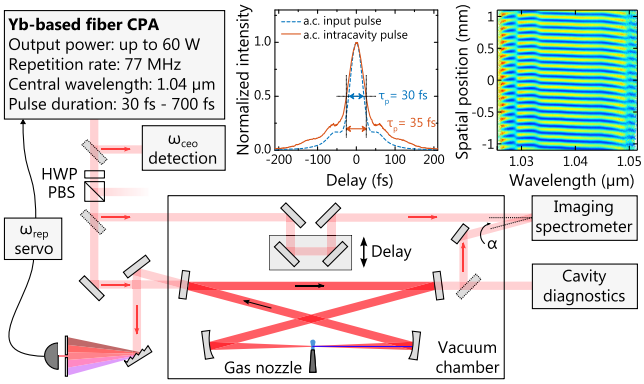

FIG. 1 (color online). Experimental setup: laser system with optional fiber broadening and compression, comb offset frequency (ω_{ceo}) detection unit, enhancement cavity ($1/e^2$ focus radius: 25 μm), active stabilization of the center frequency to the cavity resonance, and imaging spectrometer. The offset frequency of the laser is adjustable and free running. Insets: autocorrelation trace of laser and intracavity pulse for compressed input pulses and interferogram showing distinct phase jumps. HWP: half-wave plate, PBS: polarizing beam splitter.

photonic-crystal fiber and compressed via chirped mirrors to 30 fs. The pulses are coherently enhanced in a standard-approach EC. With 30-fs input pulses, an intracavity pulse duration of 35 fs at a power enhancement factor of 250 was reached, leading to an average power of 3.3 kW without a gas target.

Besides a power enhancement, the resonant cavity provides a means of enhancing the single-round-trip phase. We employ spatial-spectral interferometry to measure the spectral phase difference between the intracavity and the input pulses [2,14]. Replicas of each of these beams intersect noncollinearly at the entrance slit of an imaging spectrometer. The resulting interference pattern in the spatial and spectral plane (y,ω) is given by

$$I(y,\omega) = I_{\mathrm{in}}(y,\omega) + I_{\mathrm{cav}}(y,\omega) + 2\sqrt{I_{\mathrm{in}}(y,\omega)I_{\mathrm{cav}}(y,\omega)}\cos\left(\phi(\omega) + \frac{y\omega}{c}\sin\alpha\right). \quad (1)$$

Here, $\phi(\omega)$ is the relative spectral phase of the two pulses and α is the intersection angle of the two beams. From Eq. (1) the acquired phase $\phi(\omega)$ can be directly retrieved, without the necessity of characterizing the phases of both pulses individually. Only quadratic and higher-order terms in ω are considered, as there are multiple uncontrolled sources of group delays. Thus, a linear function must be added when comparing the retrieved phases to simulations. Both beams have to be matched in the transverse dimension and should exhibit good spatial homogeneity. When using fiber-broadened pulses this is the main source of experimental uncertainty in the retrieved phase, limiting the sensitivity to about 60 mrad. To date, spatial-spectral interferometry together with ECs has been used for measuring the single-round-trip group delay dispersion in the linear regime with a sensitivity of less than 1 fs^2 [2]. Here, we use this technique to investigate the phase modulation induced in a nonlinear interaction driven in the steady-state regime of an EC.

Our model describing the pulse propagation through the ionized medium in the cavity focus is based on the first-order propagation equation derived in Ref. [15] within the approximation of a 1D envelope description as given in Ref. [11]. In short, the nonlinear laser-gas interaction is governed by a differential equation for the pulse envelope $A(z,\tau)$ that reads in the comoving reference frame

$$\frac{dA(z,\tau)}{dz} = -\frac{I_p n}{2\epsilon_0 c}[1-\eta(z,\tau)]\Gamma_{\mathrm{peak}}(\tau)\frac{A(z,\tau)}{|A(z,\tau)|^2} + i r_e \lambda_c n \eta(z,\tau) A(z,\tau). \quad (2)$$

The first term on the right-hand side accounts for the energy loss upon ionization (I_p, ionization potential; n, gas number density; η, ionized fraction; Γ_{peak}, peak ionization rate; r_e, classical electron radius; λ_c, carrier wavelength) and the second term describes a temporal phase shift due to the rapidly changing electron density $n_e = n\eta$. Although the derivation of Eq. (2) was originally intended for pulses consisting of many cycles in the low-intensity regime, we verified that the agreement of Eq. (2) with its original counterpart (see Eq. (7) in Ref. [15]) is still excellent even for 10-fs pulses (comprising only a few cycles) and for peak intensities of 8×10^{13} W/cm^2 in a Xe gas target (see Supplemental Material [16], also for Ar and Ne).

The build-up process of the intracavity pulse is described in the frequency domain:

$$\tilde{A}_{\mathrm{cav,prior}}(\omega) = \sqrt{1-R_{\mathrm{ic}}(\omega)}\tilde{A}_{\mathrm{in}}(\omega) + \sqrt{R_{\mathrm{ic}}(\omega)R_{\mathrm{cav}}(\omega)}e^{i\phi_{\mathrm{rt}}(\omega)}\tilde{A}_{\mathrm{cav,post}}(\omega). \quad (3)$$

Here, R_{ic} is the reflectivity of the input coupler, R_{cav} represents the product of the reflectivities of all other cavity mirrors, and $\tilde{A}$ denotes the Fourier components of the field envelope (with indices for the input field and for the field before and after the plasma interaction). The spectral phase $\phi_{\mathrm{rt}}(\omega)$ is acquired upon one cavity round-trip and includes the contribution from the ionization-induced plasma. A split-step Fourier algorithm is used to solve the coupled equations (2) and (3). The employed 1D model neglects the spatial dependence of the nonlinearity and, therefore, the coupling of energy to higher-order transverse modes. Since the cavity is operated such that only the fundamental mode is resonant, transverse effects of the plasma result in additional losses and the cavity beam profile remains spatially homogeneous. This is confirmed by the imaging 2D spectrometer. For typical gas-density-length products that are below 2×10^{17} cm^{-2} and for the intensity range studied here, the 1D model is a good approximation

(see Supplemental Material [16] for comparison to 4D simulation).

All inputs to the model are taken as measured or as calculated by other independent simulations so that fit parameters are not necessary. Since the cross-sectional density of freed electrons determines the phase shift, it is essential to mimic this quantity when approximating the 2D spatial beam profile by a flattop profile with similar peak intensity. Therefore, we scale the ionization rate such that for every peak intensity it generates as many electrons within the flattop intensity profile as would have been released in the Gaussian beam profile with the original ionization rate. In contrast to earlier works [11,12], we find the Perelomov-Popov-Terent'ev model [25] averaged over the magnetic quantum number to be better suited for the intensity range under investigation, i.e., for Keldysh parameters greater than 1. In particular, using Ammosov-Delone-Krainov theory [26] underestimates the nonlinearity and thus leads to a significant overestimation of the reachable intracavity peak intensity (~25%). Whenever the consideration of subcycle ionization dynamics is necessary, we use the extension of the Perelomov-Popov-Terent'ev rate as given in Ref. [27].

From fluid flow simulations, the velocity of the gas atoms is calculated to be about 220 m/s. This is not sufficient to replace the plasma with new atoms in the interaction region (~20 μm) within one cavity round-trip time of 13 ns. Therefore the decay of the plasma is considered and modeled according to the dominant recombination mechanism via three-body collisions (see Supplemental Material [16]). However, the cavity response is mainly affected by the temporal phase shift and not by the dispersive effects of a preexisting plasma. This holds when the induced group-delay dispersion is below 0.2 fs^2 and when the depletion of the neutral gas is small ($\lesssim$15%). At the gas parameters used in the experiments, both criteria are fulfilled, rendering more detailed modeling unnecessary.

In Fig. 2(a), three examples of recorded spectra and spectral phase shifts of the intracavity pulse are presented. For the simulations, the mirror reflectivities and phases are taken from multilayer design calculations and the gas parameters are extracted from fluid flow simulations. The input pulse parameters are set as measured. For the broadband pulses, the deviation of the comb offset frequency from the value required by the cavity for optimum enhancement is particularly critical, because even deviations as small as 2 MHz from the optimum value lead to a drop in intracavity power by 50% and to a spectral filtering. The offset frequency is, however, sufficiently stable on the time scale of data acquisition, that active stabilization is not compelling (beat-note linewidth ~200 kHz, measured with a resolution bandwidth of 100 kHz). A small detuning of the locked central comb line from the empty cavity resonance is introduced avoiding the regime of optical

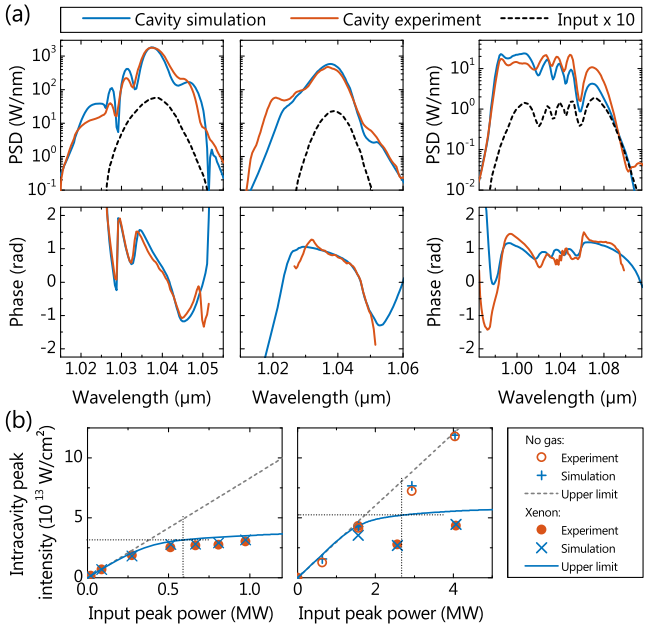

FIG. 2 (color online). Validation of the nonlinear cavity model in a standard-approach cavity. (a) Measured power spectral densities (PSD, upper panel) and acquired phases (lower panel) of the intracavity pulse along with simulation results. Left to right: input pulse duration, 640 fs (upchirped); 180 fs (Fourier limited); 30 fs (fiber broadened). Without ionization, the spectrum is symmetrically enhanced around the central wavelength. (b) Intracavity peak intensity as a function of input peak power for 640-fs (left) and for 30-fs pulses (right). The outlier in the right panel is due to an incorrectly set offset frequency of the comb. Gas density, 9×10^{18} cm^{-3}; interaction length, 180 μm; finesse, 1190 (narrowband case) and 950 (broadband case).

bistability [10,11], and keeping intracavity power fluctuations below 1% rms (band: 2.5 Hz to 5 MHz) and ensuring operation close to the maximum of the nonlinear resonance. The agreement between the simulated spectra and phases to the measured ones is excellent, validating the 1D nonlinear cavity model in a broad parameter range. Simulations yield the ionized population before the pulse and the ionization per pulse to be both on the order of 2×10^{16} cm^{-3}.

Figure 2(b) depicts the dependence of the intracavity peak intensity on the input peak power for two different pulse durations. Both curves reveal the intensity clamping behavior reported previously [9,10]. Again, the simulated intensities agree well with the experimentally determined ones. From the simulations we deduce an upper limit for the intracavity intensity [solid line in Fig. 2(b)]. This is found by optimizing the input frequency comb (ω_r, ω_{ceo}) while keeping all other parameters fixed. It has been shown that this optimum is located at nonzero detuning of the comb from the linear cavity resonances and coincides with a local bifurcation of the intracavity power at which stable operation of the cavity is impossible [11].

To optimize the nonlinear laser-gas interaction, e.g., for maximizing conversion efficiency to the XUV via HHG

[28], a simple expression relating the achievable intracavity intensity to the given cavity, gas, and input pulse parameters is desirable. To this end, we calculate the clamping behavior for a broad range of hundreds of different combinations of values for the gas parameters (density-length product, $nl = 4\text{–}20 \times 10^{16}$ cm^{-2}), the finesse ($\mathcal{F} = 250\text{–}2500$) and the pulse duration ($\tau = 12\text{–}600$ fs). Standard-approach cavities are considered: we assume a uniform mirror reflectivity, symmetric to the central wavelength and zero group delay dispersion over sufficient bandwidth to limit intracavity pulse lengthening to 1% in the absence of gas and at an input coupler transmission of 1%. Although the intracavity intensity seems to be unbound, the distinct saturation behavior motivates the definition of a clamping intensity. We find that for given gas and pulse parameters and for a targeted intensity there is an optimum cavity finesse that minimizes the required input peak power. Conversely, each finesse is optimal for a desired intensity. This intensity is reached when the peak power enhancement has dropped to about 60% to 70% of its value without a gas target. Therefore, we define the clamping intensity I_{CL} as the intracavity intensity, at which the peak power enhancement equals 65% of its linear value [see dotted cross in Fig. 2(b)]. We find that the following empirical law with the parameters α, β, γ, and δ describes the entire range of simulations within 7% of accuracy:

$$I_{\mathrm{CL}}(\tau, \mathcal{F}, nl) = I_0 \times \left(\frac{\tau_0 - \alpha}{\tau - \alpha} \frac{\mathcal{F}_0 - \beta}{\mathcal{F} - \beta} \frac{n_0 l_0 - \gamma}{nl - \gamma} \right)^{\delta}. \quad (4)$$

All coefficients are given in Table I. It is not surprising that the three input parameters pulse duration, finesse, and the gas-density-length product scale with the same exponent δ: in terms of accumulated temporal phase shift, increasing the finesse is very similar to having a longer or denser gas jet or to increasing the pulse duration. The small value of δ is a direct consequence of the high degree of nonlinearity of the ionization process. It reveals that the ionization constitutes a rather severe limit for scaling the intensity in the presence of an intracavity gas target. For instance, in the clamping regime doubling the intensity requires a decrease in any of the other parameters by roughly a factor of 90.

TABLE I. Parameters for the empirical scaling law of Eq. (4) describing the intensity clamping. $\tau_0 = 100$ fs, $\mathcal{F}_0 = 416$, and $n_0 l_0 = 8 \times 10^{16}$ cm^{-2}. Simulations were performed with a repetition rate of 100 MHz and with a gas target length of 200 μm. The bandwidth of the ECs corresponded to the input pulse durations at 1.04 μm central wavelength.

	Xenon	Argon	Neon
α (fs)	0.8	3.3	5.3
β	61	69	72
γ (10^{16}/cm^2)	0.96	0.97	1.0
δ	0.159	0.153	0.148
I_0 (10^{14} W/cm^2)	0.461	1.24	3.72

For our intensity range, the phase-modulation term in Eq. (2) is the predominant limitation. For a single pass through the gas target it takes the approximate form $\Theta(t) = r_e \lambda_c \eta(t) nl$. At the clamping limit intensity the single-pass phase shift at the end of the pulse takes the value of about $\Theta_{\max} = 6.3/\mathcal{F}$ with a minor dependence on other parameters. This is about a factor of 2 higher than the previously reported rule of thumb of $\pi/\mathcal{F}$ [12,29]. The expression for Θ and the tolerable single-pass phase shift $\Theta_{\max}$ are a good starting point for transferring our findings to other driving wavelengths, e.g., for extending the XUV cutoff wavelength (see Supplemental Material [16]).

The tradeoff between intracavity intensity and cavity finesse [see Eq. (4)] raises the question of whether parameters leading to record XUV conversion efficiencies in single-pass HHG experiments [30] can ever be reached in ECs at a reasonable power enhancement. With our experimentally validated model this question can be addressed by designing cavity mirrors to optimize the peak power enhancement in the presence of a gas target with parameters for efficient HHG [30]. In the following example, we seek for a steady-state solution of Eq. (3) presupposing the intracavity pulse $\tilde{A}_{\mathrm{cav,prior}}$ with a peak intensity of 8×10^{13} W/cm^2, from which $\tilde{A}_{\mathrm{cav,post}}$ directly follows. Using this ansatz, the input coupler reflectivity $R_{\mathrm{ic}}(\omega)$ can be calculated such that the required input power [$\propto |\tilde{A}_{\mathrm{in}}(\omega)|^2$] is minimized. In this example, we consider an EC equipped with broadband complementary-phase mirrors [31,32] supporting a bandwidth of 260 nm. The presupposed intracavity spectrum is manually varied to maximize the peak power enhancement. With the spectra shown in Fig. 3(a), a peak power enhancement surpassing 450 is possible at intracavity pulse durations of 10 fs with incident pulses as long as 52 fs. Since the intracavity

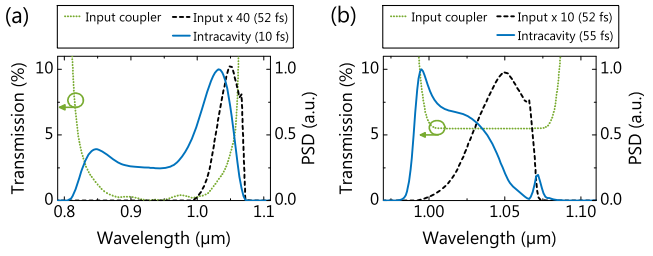

FIG. 3 (color online). (a) Example of a tailored input coupler transmission for best peak power enhancement at 8×10^{13} W/cm^2 peak intensity and corresponding intracavity and input spectrum (right y axis). Note the reduced width of the input spectrum. (b) The same input spectrum enhanced in a standard cavity requires a 10 times more powerful laser to reach the same peak intensity at 5 times longer intracavity pulses. Xe gas target length, 400 μm; particle density, 2.5×10^{18} cm^{-3}.

nonlinearity constantly transfers energy from the red part of the spectrum to the blue end, it is sufficient to pump the cavity in the long-wavelength region, in a comparatively narrow bandwidth. We verified that the solution is stable against fluctuations of up to 8% of the input power and of the pulse duration, and against a shift of the carrier wavelength of several nanometers. In contrast, enhancing the same seeding laser spectrum to the same peak intensity in a standard-approach cavity, requires 10 times the incident power and results in considerably longer intracavity pulses [see Fig. 3(b)]. The peak power enhancement and the intracavity pulse compression in the optimized EC will boost the conversion efficiency by more than 3 orders of magnitude compared to a single-pass HHG experiment using the same driving laser and by around 2 orders of magnitude compared to intracavity HHG in a standard-approach EC.

In conclusion, we have studied experimentally and theoretically the nonlinear interaction of laser pulses with a gas target in a high-finesse EC. The improved measurement sensitivity allowed for the quantitative validation of a refined nonlinear interaction model in a large parameter range. The significance of this work is twofold. First, it establishes the combination of ECs with spatial-spectral interferometry as a highly sensitive measurement technique for nonlinear light-matter interactions in general. For instance, the methodology presented here can readily be applied to χ^3 nonlinearities in bulk dielectrics. Second, our experimentally validated *ab initio* model for the nonlinear cavity response can be used in conjunction with models for phase matching in HHG [28] to globally optimize the conversion efficiency to the XUV. We show that tailoring the spectral reflectivities of EC mirrors to exploit the spectral broadening induced by the intracavity nonlinearity is a viable route towards a dramatic increase in the peak power enhancement over standard-approach ECs. In particular, a temporal compression of the intracavity pulse down to the few-cycle regime can be reached for parameters typical for phase-matched HHG. This will enable intracavity HHG experiments at similar laser pulse and gas parameters as state-of-the-art single-pass setups [30] but at significantly higher repetition rates and XUV output powers. In addition, the precise control of intracavity nonlinearities together with the increased degree of ionization tolerated by such an EC offers the prospect of generating ultrabroadband frequency combs ranging from the mid to the far-infrared via THz generation in a photo-induced plasma [33].

The authors thank M. Ciappina, Th. Udem, and A. Apolonski for helpful discussions. This work was supported by the DFG Cluster of Excellence, Munich Centre for Advanced Photonics (MAP), by the BMBF project, Photonische Nanomaterialien (PhoNa), and by the MEGAS Fraunhofer-/Max-Planck-Gesellschaft cooperation.

*simon.holzberger@mpq.mpg.de

[1] A. Foltynowicz, P. Masłowski, A. J. Fleisher, B. J. Bjork, and J. Ye, Appl. Phys. B **110**, 163 (2013).
[2] I. Pupeza, X. Gu, E. Fill, T. Eidam, J. Limpert, A. Tünnermann, F. Krausz, and T. Udem, Opt. Express **18**, 26184 (2010).
[3] T. J. Hammond, A. K. Mills, and D. J. Jones, Opt. Express **17**, 8998 (2009).
[4] H. Carstens, N. Lilienfein, S. Holzberger, C. Jocher, T. Eidam, J. Limpert, A. Tünnermann, J. Weitenberg, D. C. Yost, A. Alghamdi, Z. Alahmed, A. Azzeer, A. Apolonski, E. Fill, F. Krausz, and I. Pupeza, Opt. Lett. **39**, 2595 (2014).
[5] C. Gohle, T. Udem, M. Herrmann, J. Rauschenberger, R. Holzwarth, H. A. Schuessler, F. Krausz, and T. W. Hänsch, Nature (London) **436**, 234 (2005).
[6] R. J. Jones, K. D. Moll, M. J. Thorpe, and J. Ye, Phys. Rev. Lett. **94**, 193201 (2005).
[7] A. Cingöz, D. C. Yost, T. K. Allison, A. Ruehl, M. E. Fermann, I. Hartl, and J. Ye, Nature (London) **482**, 68 (2012).
[8] C. Benko, T. K. Allison, A. Cingöz, L. Hua, F. Labaye, D. C. Yost, and J. Ye, Nat. Photonics **8**, 530 (2014).
[9] I. Pupeza, S. Holzberger, T. Eidam, H. Carstens, D. Esser, J. Weitenberg, P. Rußbüldt, J. Rauschenberger, J. Limpert, T. Udem, A. Tünnermann, T. W. Hänsch, A. Apolonski, F. Krausz, and E. Fill, Nat. Photonics **7**, 608 (2013).
[10] D. C. Yost, A. Cingöz, T. K. Allison, A. Ruehl, M. E. Fermann, I. Hartl, and J. Ye, Opt. Express **19**, 23483 (2011).
[11] T. K. Allison, A. Cingöz, D. C. Yost, and J. Ye, Phys. Rev. Lett. **107**, 183903 (2011).
[12] D. R. Carlson, J. Lee, J. Mongelli, E. M. Wright, and R. J. Jones, Opt. Lett. **36**, 2991 (2011).
[13] T. Eidam, F. Röser, O. Schmidt, J. Limpert, and A. Tünnermann, Appl. Phys. B **92**, 9 (2008).
[14] A. P. Kovács, K. Osvay, Z. Bor, and R. Szipöcs, Opt. Lett. **20**, 788 (1995).
[15] M. Geissler, G. Tempea, A. Scrinzi, M. Schnürer, F. Krausz, and T. Brabec, Phys. Rev. Lett. **83**, 2930 (1999).
[16] See Supplemental Material at http://link.aps.org/supplemental/10.1103/PhysRevLett.115.023902, which includes Refs. [17–24], for the validity of the 1D approach and the envelope approximation and detailed information on the modelling of the plasma decay.
[17] W. H. Press, *Numerical Recipes: The Art of Scientific Computing*, 3rd ed. (Cambridge University Press, Cambridge, 2007).
[18] B. Bernhardt, A. Ozawa, A. Vernaleken, I. Pupeza, J. Kaster, Y. Kobayashi, R. Holzwarth, E. Fill, F. Krausz, T. W. Hänsch, and T. Udem, Opt. Lett. **37**, 503 (2012).
[19] Y. B. Zeldovič, Y. P. Rajzer, and W. D. Hayes, *Physics of Shock Waves and High-Temperature Hydrodynamic Phenomena* (Dover Publication, Mineola and New York, 2002).
[20] E. P. Kanter, R. Santra, C. Höhr, E. R. Peterson, J. Rudati, D. A. Arms, E. M. Dufresne, R. W. Dunford, D. L. Ederer, B. Krässig, E. C. Landahl, S. H. Southworth, and L. Young, J. Appl. Phys. **104**, 073307 (2008).
[21] E. Hinnov and J. Hirschberg, Phys. Rev. **125**, 795 (1962).
[22] M. C. M. van de Sanden, J. M. de Regt, and D. C. Schram, Phys. Rev. E **47**, 2792 (1993).

[23] L. Allen, D. G. C. Jones, and D. G. Schofield, J. Opt. Soc. Am. **59**, 842 (1969).
[24] M. R. Bruce, W. B. Layne, C. A. Whitehead, and J. W. Keto, J. Chem. Phys. **92**, 2917 (1990).
[25] A. M. Perelomov, V. S. Popov, and M. V. Terent'ev, Zh. Eksp. Teor. Fiz. **50**, 1393 (1966) [Sov. Phys. JETP **23**, 924 (1966)].
[26] M. V. Ammosov, N. B. Delone, and V. P. Krainov, Zh. Eksp. Teor. Fiz. **91**, 2008 (1986) [Sov. Phys. JETP **64**, 1191 (1986)].
[27] G. L. Yudin and M. Y. Ivanov, Phys. Rev. A **64**, 013409 (2001).
[28] S. Kazamias, S. Daboussi, O. Guilbaud, K. Cassou, D. Ros, B. Cros, and G. Maynard, Phys. Rev. A **83**, 063405 (2011).
[29] K. D. Moll, R. J. Jones, and J. Ye, Opt. Express **13**, 1672 (2005).
[30] S. Hädrich, A. Klenke, J. Rothhardt, M. Krebs, A. Hoffmann, O. Pronin, V. Pervak, J. Limpert, and A. Tünnermann, Nat. Photonics **8**, 779 (2014).
[31] F. X. Kärtner, U. Morgner, R. Ell, T. Schibli, J. G. Fujimoto, E. P. Ippen, V. Scheuer, G. Angelow, and T. Tschudi, J. Opt. Soc. Am. B **18**, 882 (2001).
[32] V. Pervak, A. V. Tikhonravov, M. K. Trubetskov, S. Naumov, F. Krausz, and A. Apolonski, Appl. Phys. B **87**, 5 (2007).
[33] E. Matsubara, M. Nagai, and M. Ashida, J. Opt. Soc. Am. B **30**, 1627 (2013).